# Investigation of the inhibitory activity of some 3-aryl(hetaryl)-5-amino-1*H*-1,2,4-triazoles on copper chloride corrosion

## D.V. Lyapun, A.A. Kruzhilin, D.S. Shevtsov and Kh.S. Shikhaliev*

*Voronezh State University, 1 Universitetskaya pl., 394018 Voronezh, Russian Federation*
*\*E-mail: shikh1961@yandex.ru*

## Abstract

The article describes an example of applying the principles of molecular design to develop new organic corrosion inhibitors. Methods for the synthesis of 3-aryl/hetaryl-5-amino-1*H*-1,2,4-triazoles have been developed, and the influence of substituent nature at the 3rd position in the molecules of 1,2,4-triazoles on their inhibitory activity towards copper corrosion in chloride solutions (1% HCl) has been investigated. The research on a series of 3-aryl/hetaryl derivatives of 5-amino-1,2,4-triazole revealed that the anti-corrosive properties of substances in this class substantially depend on the structure of the aromatic substituent. Direct corrosion tests in chloride solutions have shown that 3-(pyridin-3-yl)-1*H*-5-amino-1,2,4-triazole **2d** and 3-(thiophen-2-yl)-1*H*-5-amino-1,2,4-triazole **2f**, at a concentration of 0.01M, provide copper protection levels of 87.7% and 85.9%, respectively. We suggest that the maximum protective effect of pyridin-3-yl-5-amino-1,2,4-triazole **2d** is due to the fact that the pyridine, attached to the basic triazole matrix in the 3rd position, acts as a strong electron density acceptor, increasing the acidity of the nitrogen endo-atom in the triazole and facilitating the formation of more stable complexes with copper atoms. Quantum chemical calculations revealed that the presence of a pyridin-3-yl substituent in the structure of aminotriazole leads to the lowest values of HLG, which is also considered indirect evidence of high protective properties in homologous series of inhibitors adsorbed on the metal surface. The high protective effect of pyridin-3-yl-5-amino-1,2,4-triazole was demonstrated using SEM microscopy.

## 1. Introduction

Copper and its alloys are actively used in various industries such as construction, transportation, energy, microelectronics, light and heavy industries, serving as material for heat exchange equipment, structural elements, roofing materials, plumbing systems, conductors, and electrical equipment components. One of the most effective methods to reduce its corrosion damage involves the use of corrosion inhibitors. These substances provide stability to copper and its alloys against corrosion caused by various factors such as weather conditions, humidity, chloride content, petroleum products, high temperatures, aggressive gases, chemicals, and liquids. Azoles and their derivatives have gained

widespread acceptance in protecting copper and its alloys from corrosion [1−4]. Recently, they have been receiving more attention as the successful selection of substituents can broaden or, conversely, specify the application area of the obtained inhibitor [5−7].

It is worth noting separately that heterocyclic compounds are frequently used as physiologically and biologically active compounds, constituting medicinal preparations and natural compounds. Often, the introduction of heterocyclic or aromatic substituents into the structure of an organic compound allows for the emergence of similar properties, such as antiviral, antimicrobial, bactericidal, antifungal activities, and so forth [8, 9]. In this regard, the presence of such substituents in the structure of corrosion inhibitors may contribute to both the enhancement of protective properties and the imparting of additional beneficial properties, such as bactericidal effects to inhibit bacterial corrosion [10, 11].

Earlier, the authors of this paper have already published research results on other derivatives of aminotriazoles concerning their anti-corrosion activity on copper. These include 3-alkyl- [12], 3-alkylmercapto- [13], *N*-substituted piperidinyl-, morpholinyl-, pyrrolidinyl- derivatives of aminotriazoles [14], as well as triazolopyrimidines and triazolotriazines obtained based on aminotriazoles [15], among others. This article is dedicated to developing synthesis methods for 3-aryl/hetaryl-5-amino-1*H*-1,2,4-triazoles and investigating the influence of substituents in the 3rd position in the molecules of 1,2,4-triazoles on their inhibitory activity towards copper chloride corrosion.
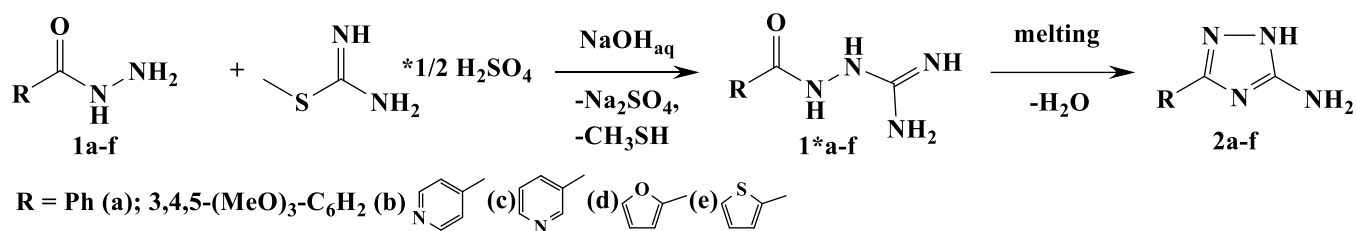
## 2. Experimental

### 2.1. Methods for analyzing the chemical structure and composition of inhibitors

For the analysis of aminotriazoles, high-performance liquid chromatography with high-resolution mass spectrometric detection using electrospray ionization (HPLC-HRMS-ESI) combined with UV detection was employed. The setup consisted of an Agilent 1269 Infinity liquid chromatograph and an Agilent 6230 TOF LC/MS time-of-flight mass detector. Quantitative determination was performed using the internal standard method. $^1$H NMR spectra were recorded on a Bruker AV600 spectrometer (600.13 MHz) in DMSO-$d_6$, with TMS used as an internal standard. IR spectra were recorded on a Vertex 70 Fourier-transform infrared spectrometer equipped with a Platinum ATR accessory (Bruker), featuring a diamond prism, in the frequency range from 4000 to 400 cm$^{-1}$ with a resolution of 2 cm$^{-1}$. The result was obtained by averaging 16 scans.

### 2.2. Synthesis and analysis of inhibitors

The study investigated a method for obtaining derivatives of aminotriazole, where aromatic or heteroaromatic substituents are introduced in the third position of the heterocycle. This method involves the interaction of respective aroyl or hetaroyl hydrazides with *S*-methylisothiourea hemisulfate in the presence of a base.

R = Ph (a); 3,4,5-(MeO)₃-C₆H₂ (b) (c) (d) (e)

The starting aroyl hydrazides **1a–b** and hetaroyl hydrazides **1c–f** were obtained using a known method [16, 17], involving the interaction of corresponding benzoyl and hetaroyl carboxylic acid esters with a 1.5-fold excess of hydrazine hydrate. We found that the optimal conditions for the interaction of the obtained hydrazides with *S*-methylisothiourea hemisulfate involve conducting the process at room temperature in aqueous alkaline solution. To increase the yield of the final product, the reaction mixture was heated to ~100°C for half an hour after the intensive evolution of methyl mercaptan ceased. As a result, the yield of intermediate aroyl(hetaroyl) amidinohydrazides was increased approximately two-fold (60–70% instead of 30–40%) compared to the original method [18].

The obtained aroyl(hetaroyl)amidinohydrazides were subjected to intramolecular heterocyclization in the second stage, which occurred upon melting and holding at a temperature of 250–300°C for 3–5 minutes. Under these conditions, nucleophilic attack by the carbon atom of the carbonyl group of the amidine moiety of the guanidine fragment takes place, resulting in the liberation of water and the formation of a 1,2,4-triazole ring.

Thus, a series of previously unstudied 3-aryl/hetaryl-5-amino-1*H*-1,2,4-triazoles were obtained and subsequently investigated as inhibitors of copper chloride corrosion (Table 1).

**Table 1.** List of inhibitors studied.

| Symbol | Name | Formula |
|---|---|---|
| **2a** | 3-Phenyl-1*H*-1,2,4-triazol-5-amine |  |
| **2b** | 3-(3,4,5-Trimethoxyphenyl)-1*H*-1,2,4-triazol-5-amine |  |
| **2c** | 3-(Pyridin-4-yl)-1*H*-1,2,4-triazol-5-amine |  |
| **2d** | 3-(Pyridin-3-yl)-1*H*-1,2,4-triazol-5-amine |  |

| Symbol | Name | Formula |
|--------|------|---------|
| **2e** | 3-(Furan-2-yl)-1*H*-1,2,4-triazol-5-amine |  |
| **2f** | 3-(Thiophen-2-yl)-1*H*-1,2,4-triazol-5-amine |  |

*General procedure for the synthesis of 3-aryl-5-amino-1H-1,2,4-triazoles 2a-b and 3-hetaryl-5-amino-1H-1,2,4-triazoles **2c−e**.*

To 0.1 mol of *S*-methylisothiourea hemisulfate, 100 ml of 1 M NaOH was added with stirring and cooling, followed by the addition of 0.1 mol of aroyl hydrazide. The mixture was left at room temperature for 24 hours. Then the mixture was heated to the boiling point of the solvent and maintained under these conditions for 30−60 minutes. The resulting mixture was cooled, filtered, and washed with distilled water. The obtained precipitate was dried and subjected to melting at a temperature of 250−300°C. The solid residue was ground in a mortar. The obtained substances were recrystallized from a mixture of ethyl acetate/methanol.

3-Phenyl-1*H*-1,2,4-triazol-5-amine **2a**. Yield 65%, white solid, m.p. 178−180°C. 6.02 (s, 2H, $NH_2$), 7.21−7.49 (m, 3H, $CH_{arom}$), 8.22 (d, 2H, $CH_{arom}$), 12.23 (br.s, H, NH). Found, *m/z*: 161.0711 $[M+H]^+$. $C_5H_8N_8S_2$. Calculated, *m/z*: 161.0749.

3-(3,4,5-Trimethoxyphenyl)-1*H*-1,2,4-triazol-5-amine **2b**. Yield 61%, white solid, m.p. 138−140°C. 3.72 (s, 9H, $3OCH_3$), 6.05 (s, 2H, $NH_2$), 7.06 (s, 2H, $CH_{arom}$), 12.14 (br.s, H, NH). Found, *m/z*: 251.1124 $[M+H]^+$. $C_5H_8N_8S_2$. Calculated, *m/z*: 251.1066.

3-(Pyridin-4-yl)-1*H*-1,2,4-triazol-5-amine **2c**. Yield 72%, white solid, m.p. 270–272°C. 6.22 (s, 2H, $NH_2$), 7.77 (d, 2H, $CH_{arom}$), 8.18 (d, 1H, $CH_{arom}$), 8.54 (d, 1H, $CH_{arom}$), 9.06 (s, 1H, $CH_{arom}$), 12.23 (br.s, H, NH). Found, *m/z*: 162.1835 $[M+H]^+$. $C_5H_8N_8S_2$. Calculated, *m/z*: 162.0701.

3-(Pyridin-3-yl)-1*H*-1,2,4-triazol-5-amine **2d**. Yield 75%, white solid, m.p. 244–246°C. 6.17 (s, 2H, $NH_2$), 7.43 (t, *J*=4.9, 1H, $CH_{arom}$), 8.60 (d, 2H, $CH_{arom}$), 12.36 (br.s, H, NH). Found, *m/z*: 162.0920 $[M+H]^+$. $C_5H_8N_8S_2$. Calculated, *m/z*: 162.0701.

3-(Furan-2-yl)-1*H*-1,2,4-triazol-5-amine **2e**. Yield 71%, white solid, m.p. 182−184°C. 5.92 (s, 2H, $NH_2$), 7.21 (t, 1H, $CH_{furan}$), 7.48 (d, 1H, $CH_{furan}$), 8.15 (d, 1H, $CH_{furan}$), 12.41 (br.s, H, NH). Found, *m/z*: 151.0825 $[M+H]^+$. $C_5H_8N_8S_2$. Calculated, *m/z*: 151.0542.

3-(Thiophen-2-yl)-1*H*-1,2,4-triazol-5-amine **2f**. Yield 67%, white solid, m.p. 200–202°C. 6.20 (s, 2H, $NH_2$), 7.73 (t, 1H, $CH_{thiophene}$), 8.08 (d, 1H, $CH_{thiophene}$), 8.35 (d, 1H, $CH_{thiophene}$), 12.29 (br.s, H, NH). Found, *m/z*: 167.0532 $[M+H]^+$. $C_5H_8N_8S_2$. Calculated, *m/z*: 167.0313.

To assess the protective action of the synthesized compounds (**2a−2f**), a combination of electrochemical and direct corrosion methods was employed.

## 2.3. *Potentiodynamic polarization measurements*

Electrochemical measurements were conducted at room temperature (approximately 25°C) on copper electrodes M1 (copper content not less than 99.9%) in an immiscible borate buffer aqueous solution (pH 7.4) under natural aeration conditions in the presence of the inhibitor and activating additive 10 mM sodium chloride in a three-electrode electrochemical cell with undivided electrode compartments to enhance the speed of non-stationary measurements.

The saturated silver chloride reference electrode was placed in a separate vessel connected to the electrochemical cell by means of an agar-agar-based electrolytic bridge, filled with a saturated solution of potassium nitrate. The auxiliary electrode was a platinum mesh. The working copper electrode was pre-cleaned with 3000-grit sandpaper, degreased with 96% ethanol, and rinsed with distilled water. The potentials of the working electrode ($E$) are reported relative to the standard hydrogen electrode (SHE) scale. The current density ($i_{cor}$) was calculated by dividing the registered current strength ($I$) by the geometric area of the working electrode (0.75 cm$^2$).

Measurements were carried out using the IPC-PRO potentiostat. To remove the oxide film formed in the air, the working Cu electrode was cathodically pre-polarized at $E=-0.60$ V for 15 minutes, after which polarization was turned off, and the electrode was kept in the solution until the establishment (within 3−5 minutes) of a stationary value of the open circuit potential ($E_{cor}$). Then, a solution of NaCl was introduced into the working solution with stirring to provide a chloride ion concentration $C_{Cl^-}=10$ mmol/dm$^3$, as well as the investigated inhibitors at concentrations of $C_{inh}=0.01, 0.10$, or $1.00$ mmol/dm$^3$. After the establishment of the new $E_{cor}$ value, a polarization curve was recorded by scanning the potential in the anodic or cathodic direction at a rate of 0.2 mV/s. The pitting potential ($E_p$) was determined by the sharp increase in current on the anodic polarization curve followed by visual identification of pitting on the electrode surface.

## 2.4. *Direct corrosion tests*

Gravimetric corrosion tests were conducted on copper plates measuring $20\times50\times0.10$ mm, which were previously polished with K3000 sandpaper and degreased with acetone. Experiments were carried out for 7 days simultaneously on three samples in an unmixed, naturally aerated 1 mass% aqueous solution of HCl with or without the addition of the investigated inhibitors. After the experiments, the plates were rinsed with distilled water and processed according to the requirements of GOST 9.907-83 "Methods of Utilization of Products after Corrosion Tests." The corrosion rate was determined by the mass loss of the samples and calculated using the equation:

$$k_{inh} = \frac{m_0 - m}{s \cdot t}$$

where $m_0$ and $m$ are the mass of the sample before and after corrosion testing, respectively, in grams, $S$ is the geometric area of the plate in square meters, and $t$ is the duration of the experiment in days.

The inhibition efficiency was assessed based on the degree of protection value:

$$Z_{\text{k}} = \frac{k_0 - k_{\text{inh}}}{k_0} \cdot 100\% \, ,$$

where $k_0$ and $k_{\text{inh}}$ are the corrosion rates in the HCl solution without inhibitor and with an inhibitor, respectively. The value of the $k_0$ parameter was ~$19.2$ g·m$^{-2}$·day$^{-1}$.

Atmospheric corrosion of copper was accelerated by testing in a salt spray chamber to determine the effectiveness of inhibiting 3-aryl/hetaryl-5-amino-1*H*-1,2,4-triazoles in the interoperation protection of copper products. Protective inhibitor films were obtained by immersing copper plates in an aqueous solution with the inhibitor for 60 minutes at 60°C. The samples were wiped with filter paper and air-dried at room temperature for 2 hours, then placed in a sealed chamber with a volume of 14000 cm$^3$ and 95−100% air humidity. A 5 wt.% NaCl solution was sprayed into the chamber using a pump with 6 hydraulic nozzles by automatically activating it for 1 second every hour (solution flow rate per nozzle ~7 ml). The samples were inspected 3 times a day to determine the time of appearance of the first signs of corrosion ($\tau_{\text{cor}}$)

### 2.5. Quantum chemical calculations

All synthesized molecules were fully optimized using density functional theory (DFT) with the B3LYP functional and the 6-31G++(d,p) basis set in the Gaussian program [19]. The optimized geometry exhibits non-negative frequencies, indicating that the molecules are situated with minimum energy on the potential energy surface. The determination of HOMO, LUMO energies, and the HOMO-LUMO gap, as well as ionization potential (*IP*), electron affinity (*EA*), electronegativity ($\chi$), absolute hardness ($\eta$), and softness ($\sigma$) for all molecules, was performed at the same level of theory.

According to density functional theory, absolute hardness ($\eta$) is defined as [20].

$$\eta = \frac{1}{2}\frac{\partial \mu}{\partial N} = \frac{1}{2}\frac{\partial^2 E}{\partial N^2}$$

where $\mu$ is the chemical potential, $N$ is the number of electrons, and $E$ is the energy. R.G. Pearson proposed the operational definition of absolute hardness as

$$\eta = \frac{IP - EA}{2}$$

where *IP* and *EA* represent ionization energy and electron affinity, respectively. Additionally, according to Koopmans' theorem, from the orbital basis, *IP* and *EA* are determined as

$$IP = -E_{\text{HOMO}} \, ; \; EA = -E_{\text{LUMO}}$$

$E_{\text{HOMO}}$ and $E_{\text{LUMO}}$ are the energies of the highest occupied and lowest unoccupied molecular orbitals, respectively. From the formula above, hardness is a measure of the stability against
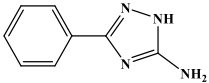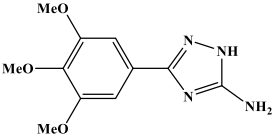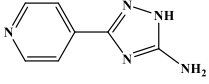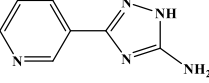
changes in the electron cloud of the chemical system. Softness ($\sigma$) is inversely proportional to hardness, an important parameter in the field of reaction chemistry, as most reactive species have higher softness values. Electronegativity ($\chi$) is also defined in terms of the energies of HOMO and LUMO as
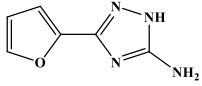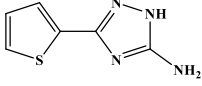
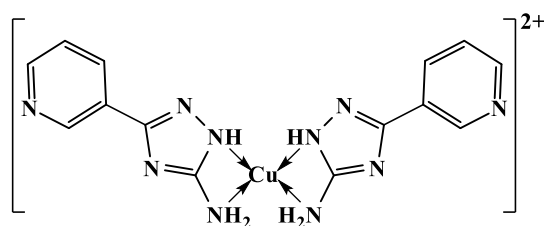$$\chi = \frac{IP + EA}{2}$$

## 3. Results and Discussion

Based on experiments in 1% HCl solutions, it was found that aminotriazoles containing an aryl substituent in their structure exhibited low levels of corrosion protection. However, in the case of hetaryl derivatives, the passivating activity significantly increased. Compounds containing a heterocyclic substituent at the 3rd position of the aminotriazole ring showed higher degrees of protection compared to aryl derivatives **2a,b**. The furan-2-yl and pyridin-4-yl derivatives **2e** and **2c**, respectively, exhibited modest protective levels at around 40–50% protection. Meanwhile, for the pyrimidin-3-yl and thiophen-2-yl-5-aminotriazoles **2d** and **2f**, respectively, the protection values were the highest among those studied and were close to 80% at the highest concentrations of 0.01 mol/L.

**Table 2.** Results of corrosion inhibition tests of 3-aryl/hetaryl-1*H*-1,2,4-triazoles using gravimetric testing methods and salt spray tests.

| Inhibitor | $C_{inh}$, mmol/dm³ | $k_{inh}$ | $Z_k$, % | $\tau_{cor}$, h |
|---|---|---|---|---|
| None | – | 19.2 | – | 2 |
| | 10.00 | 11.7 | 39.3 | 26 |
| | 1.00 | 13.4 | 30.1 | 26 |
| **2a** | 0.10 | 14.8 | 22.8 | 34 |
| | 10.00 | 16.1 | 16.0 | 18 |
| | 1.00 | 16.9 | 12.2 | 20 |
| **2b** | 0.10 | 19.0 | 0.9 | 26 |
| | 10.00 | 8.0 | 58.1 | 70 |
| | 1.00 | 11.1 | 42.0 | 66 |
| **2c** | 0.10 | 11.7 | 39.1 | 46 |
| | 10.00 | 2.4 | 87.7 | 100 |
| | 1.00 | 5.2 | 73.0 | 98 |
| **2d** | 0.10 | 4.5 | 76.6 | 94 |

| Inhibitor | $C_{inh}$, mmol/dm$^3$ | $k_{inh}$ | $Z_k$, % | $\tau_{cor}$, h |
|---|---|---|---|---|
| (structure) 2e | 10.00 | 10.2 | 47.1 | 44 |
| | 1.00 | 13.9 | 27.6 | 40 |
| | 0.10 | 11.5 | 40.2 | 38 |
| (structure) 2f | 10.00 | 2.7 | 85.9 | 44 |
| | 1.00 | 14.3 | 25.8 | 42 |
| | 0.10 | 13.2 | 31.2 | 38 |

In the course of the research, the times of appearance of initial corrosion signs were obtained for all investigated inhibitors in the salt spray chamber. The best performance at ~100 hours was also observed for compound **2d** at concentrations of 0.001–0.01 M. We hypothesize that the best obtained protective action of pyridin-3-yl-5-amino-1,2,4-triazole **2d** is associated with the pyridine moiety, attached to the basic triazole matrix at position 3, acting as a strong electron density acceptor, increasing the acidity of the nitrogen endo-atom in the triazole, and facilitating the formation of more stable complexes with dissolved copper atoms [21–23]. The probable structure of the formed copper complexes is depicted in the scheme.



In order to gain a better understanding of the inhibition mechanism and effectiveness of the investigated substances, for those identified as most effective in direct inhibition tests, **2c−f**, electrochemical potentiometric tests were conducted to obtain cathodic and anodic polarization curves. The polarization curves obtained on copper in solutions containing additives of the investigated compounds are presented in Figure 1.

**Table 3.** Results of $E_{cor}$ measurement for solutions containing inhibitors **2c−f**.

| Inhibitor/$C_{inh}$ | $E_{cor}$, mV | | | |
|---|---|---|---|---|
| | 0.00 mmol/dm$^3$ | 0.01 mmol/dm$^3$ | 0.10 mmol/dm$^3$ | 1.00 mmol/dm$^3$ |
| **2c** | +176 | +141 | +151 | +146 |
| **2d** | +176 | +151 | +191 | +161 |
| **2e** | +176 | +131 | +156 | +151 |
| **2f** | +176 | +201 | +251 | +301 |

Upon addition of 3-(pyridin-4-yl)-5-amino-1*H*-1,2,4-triazole **2c** at a concentration of 0.01 mmol/L, a shift in $E_{cor}$ of +65 mV in the anodic direction was observed, while at a concentration of 0.10 mmol/L, the shift was −25 mV in the cathodic direction. At a concentration of 1.00 mmol/L, a shift in $E_{cor}$ of −30 mV in the cathodic direction was noted (Table 3).

On the initial segment of the anodic polarization curve at a concentration of 0.01 mmol/L, the current density was lower compared to the control experiment up to a potential of ~+250 mV. At a concentration of 0.10 mmol/L, the current density on the initial segment exceeded the values of the control experiment. Further polarization led to a significant increase in the anodic current density, exceeding the maximum value of the control experiment. The passivation current density for a concentration of 0.01 mmol/L was four times higher compared to the control experiment, while for concentrations of 0.10 and 1.00 mmol/L, it practically coincided with the control. The maximum anodic current for a concentration of 0.01 mmol/L was shifted by +30 mV in the anodic direction relative to the control experiment, and for a concentration of 0.10 mmol/L, it was shifted by −90 mV in the cathodic direction. At a concentration of 1.00 mmol/L, the polarization curve coincided with the control up to the activation potential within the experimental error. The electrode potential at which the anodic current sharply increased was shifted towards the anodic region by +115, +200, and +400 mV, respectively, for concentrations of 0.01, 0.10, and 1.00 mmol/L. However, no visible pitting on the electrode surface was observed.

The cathodic polarization curve upon addition of 0.01 mmol/L of 3-(pyridin-4-yl)-5-amino-1*H*-1,2,4-triazole **2c** coincided with the control within the experimental error. For additions of 0.10 mmol/L and 1.00 mmol/L of 3-(pyridin-4-yl)-5-amino-1*H*-1,2,4-triazole, an expansion of the region of small cathodic currents was observed (the polarization curve was close to the zero current axis). For these concentrations, the position of the region of increasing cathodic current density was shifted towards the cathodic region by −100 mV relative to the control experiment.

Upon addition of 3-(pyridin-3-yl)-5-amino-1*H*-1,2,4-triazole 2d at a concentration of 0.01 mmol/L, a shift in $E_{cor}$ by −25 mV in the cathodic direction was observed, while at a concentration of 0.10 mmol/L, it shifted by +15 mV in the anodic direction. At a concentration of 1.00 mmol/L, the shift in $E_{cor}$ was −15 mV in the cathodic direction (see Table 3).

A sharp increase in the density of the anodic current was observed at the initial part of the anodic curve for all investigated additive concentrations. With further polarization, there was an intense increase in the density of the anodic current, surpassing the control value at its maximum point. The maximum anodic current for additive concentrations of 0.01, 0.10, and 1.00 mmol/L was shifted relative to the control experiment by −10, −50, and −70 mV in the cathodic direction, respectively. The current density at the maximum for concentrations of 0.01 and 0.10 mmol/L was up to four times higher compared to the control experiment, while for a concentration of 1.00 mmol/L, it practically coincided with the control experiment. The pitting potential, at which the anodic current sharply increased, was
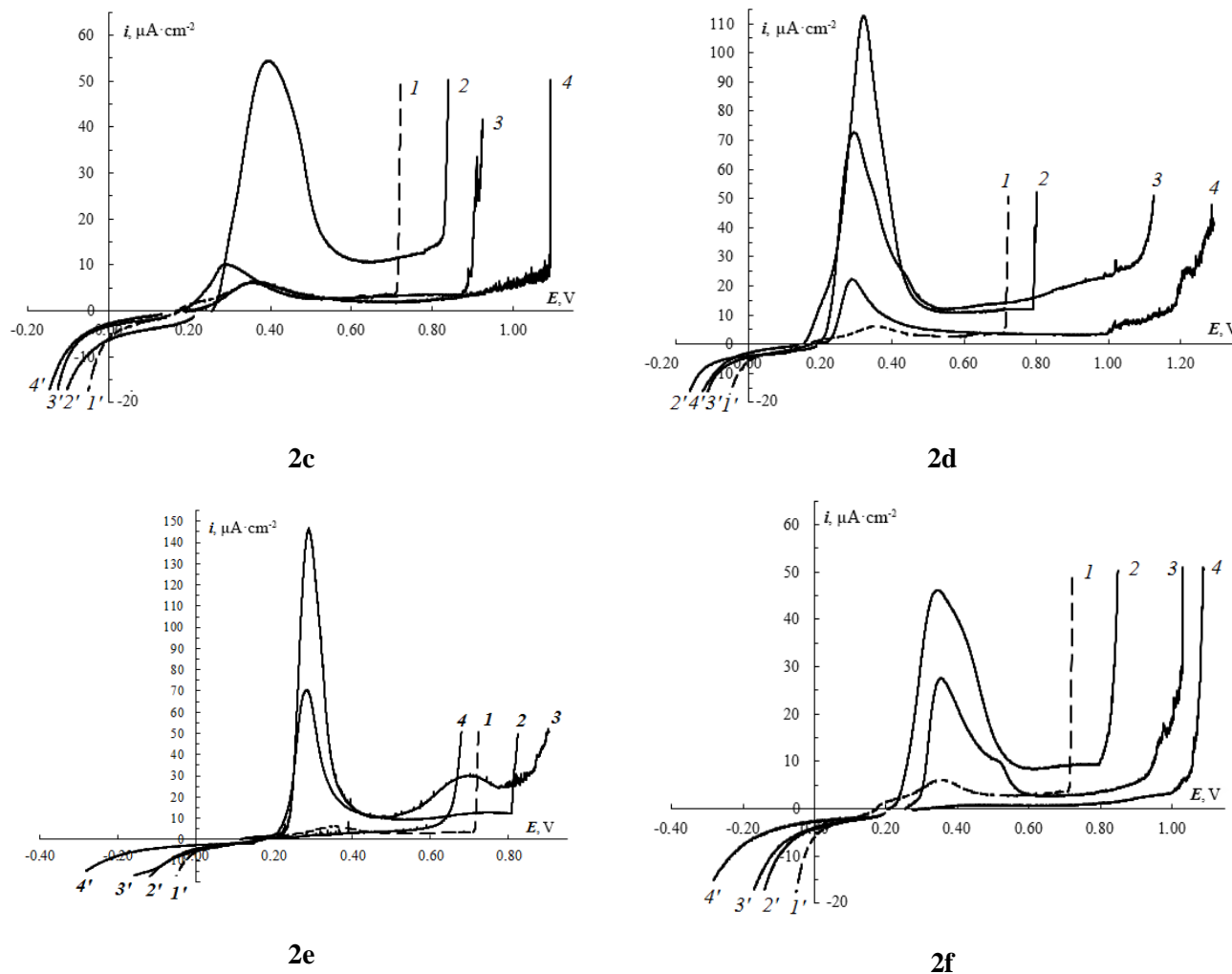
**2c**

**2d**

**2e**

**2f**

**Figure 1.** Anodic $(1-4)$ and cathodic $(1'-4')$ polarization curves obtained on copper in borate buffer (pH=7.40) with the addition of 0.01 M NaCl and inhibitors 2c−2f at concentration $C_{inh}$ (mmol/L): 1, 1′ – without additives; 2, 2′ – 0.01; 3, 3′ – 0.10; 4, 4′– 1.00.

shifted towards the anodic region by +80 mV relative to the control experiment for concentrations of 0.01 mmol/L. For additives of 0.10 and 1.00 mmol/L, a significant increase in current density was observed in the potential range of 1100−1400 mV, *i.e.*, above the control experiment by +400 and +700 mV, respectively. However, no visible pitting was observed on the electrode surface without increasing potential.

On the cathodic polarization curve at a concentration of 0.01 mmol/L of aminotriazole 2d, an expansion of the region of small cathodic currents was observed (the polarization curve was pressed to the zero current axis). The position of the region of increased cathodic current density was shifted by −150 mV relative to the control experiment. For concentrations of 0.10 and 1.00 mmol/L, the cathodic curves were practically indistinguishable, with the position of the region of increased cathodic current density shifted by −70 mV relative to the control experiment.

Upon addition of 3-(furan-2-yl)-5-amino-1*H*-1,2,4-triazole **2e** at a concentration of 0.01 mmol/L, a shift in $E_{cor}$ by −45 mV in the cathodic direction was observed, while at a concentration of 0.10 mmol/L, the shift was −20 mV towards the cathodic side. For a concentration of 1.00 mmol/L, the shift in $E_{cor}$ was noted to be −25 mV in the cathodic direction (see Table 3).

On the initial segments of the anodic polarization curves for concentrations of the additive at 0.01 and 0.10 mmol/L, the current density was higher compared to the control experiment, while at a concentration of 1.00 mmol/L, low current values were observed up to a potential of ~+470 mV. With further polarization, an intense increase in the anodic current density was observed for concentrations of the additive at 0.01 and 0.10 mmol/L, exceeding the maximum point of the control value. The maximum anodic current for a concentration of the additive at 0.01 mmol/L was shifted by −50 mV in the cathodic direction relative to the control experiment, and for a concentration of 0.10 mmol/L, it was shifted by −40 mV towards the cathodic side. No maximum was observed on the anodic polarization curve for a concentration of 1.00 mmol/L. The current density at the maximum for a concentration of 0.01 mmol/L was up to four times higher than that of the control experiment, and for a concentration of 0.10 mmol/L, it was up to five times higher. The electrode potential at which the anodic current sharply increased was shifted towards the anodic region by ~+100 mV for a concentration of 0.01 mmol/L, towards the cathodic region by ~70 mV for a concentration of 1.00 mmol/L, and for a concentration of 0.10 mmol/L, the increase started at a potential of +500 mV, passing through a peak, and reaching maximum values at $E > 800$ mV. No visible pitting on the electrode surface was observed.

On the cathodic polarization curves, an expansion of the region of small cathodic currents (the polarization curve is approaching the zero current axis) was noted. The polarization curves obtained at concentrations of the additive at 0.01 and 0.10 mmol/L were practically indistinguishable and coincided with the control on the initial segment. The position of the region of increasing cathodic current density was shifted by −100 mV relative to the control experiment for a concentration of 1.00 mmol/L, the position was shifted by −200 mV. The protective action of 3-(furan-2-yl)-5-amino-1*H*-1,2,4-triazole may manifest at concentrations below 1.00 mmol/L.

Upon addition of 3-(2-thienyl)-5-amino-1*H*-1,2,4-triazole **2f** at a concentration of 0.01 mmol/L, a shift in the $E_{cor}$ in the anodic direction by +25 mV was observed, while at a concentration of 0.10 mmol/L, the shift was +75 mV. At a concentration of 1.00 mmol/L, the $E_{cor}$ shifted in the anodic direction by +125 mV (Table 3).

At the initial segments of the anodic polarization curves for concentrations of the additive of 0.01 and 0.10 mmol/L, a decrease in current density relative to the control experiment was observed until the potentials of ~+230 and +300 mV, respectively. With further polarization, there was an intense increase in anodic current density, exceeding the maximum value observed in the control experiment. The maximum anodic current for a concentration of 0.01 mmol/L shifted towards the cathodic side by −10 mV relative to the

control experiment, while for a concentration of 0.10 mmol/L, it coincided with the position of the maximum in the control experiment. For a concentration of 1.00 mmol/L, the current density was lower than that of the control experiment over the entire potential range, and no current maximum was observed. The passivation current density for a concentration of 0.01 mmol/L was up to five times higher than that of the control experiment, practically coincided with the control for a concentration of 0.10 mmol/L, and was up to four times lower for 1.00 mmol/L. The potential at which the anodic current sharply increased was shifted towards the anodic region by +80, +200–300, and +300–350 mV, respectively, for concentrations of 0.01, 0.10, and 1.00 mmol/L. However, no visible pitting was observed on the electrode surface.

On the cathodic polarization curves, an expansion of the region of small cathodic currents was observed (the polarization curve was pressed against the zero current axis). The polarization curves obtained at concentrations of additive 0.01 and 0.10 mmol/L were practically indistinguishable. The position of the region of increasing cathodic current density was shifted by −150 mV relative to the control experiment for concentrations of 0.01 and 0.10 mmol/L, and by −200 mV for a concentration of 1.00 mmol/L.

Thus, in our case, from the point of view of describing the corrosion processes occurring on the electrode, the most indicative criterion was found to be the $E_p$ parameter characterizing pitting corrosion processes. From the obtained polarization curves, it can be seen that the shift in $E_p$ correlates with the experimentally found degrees of inhibitor protection in gravimetric experiments: the $E_p$ and $Z_k$ values decrease in the series **2d** > **2f** > **2c** > **2e**. Moreover, with an increase in the inhibitor concentration, the $E_p$ values also increase. It should be noted that at the same time, there is a proportional increase in the maximum anodic current density in the range of 0.2–0.4 V, which decreases with increasing inhibitor concentration. Presumably, the addition of all the investigated compounds contributes to the intensification of copper oxide formation processes occurring in this potential range [24].

Quantum chemical calculations were performed for all investigated compounds using the molecular mechanics method (DFT with the B3LYP 6,31g++(d,p) basis).

The calculation results (Table 4) show that the HOMO-LUMO gap (HLG) has the smallest value for compounds **2a** and **2d**. According to existing notions, this may indicate the better ability of these substances to adsorb on the surface of copper, and therefore, better protective characteristics. Thus, quantum chemical calculations correlate with the results obtained in direct corrosion studies, except for the data for compound **2a**.
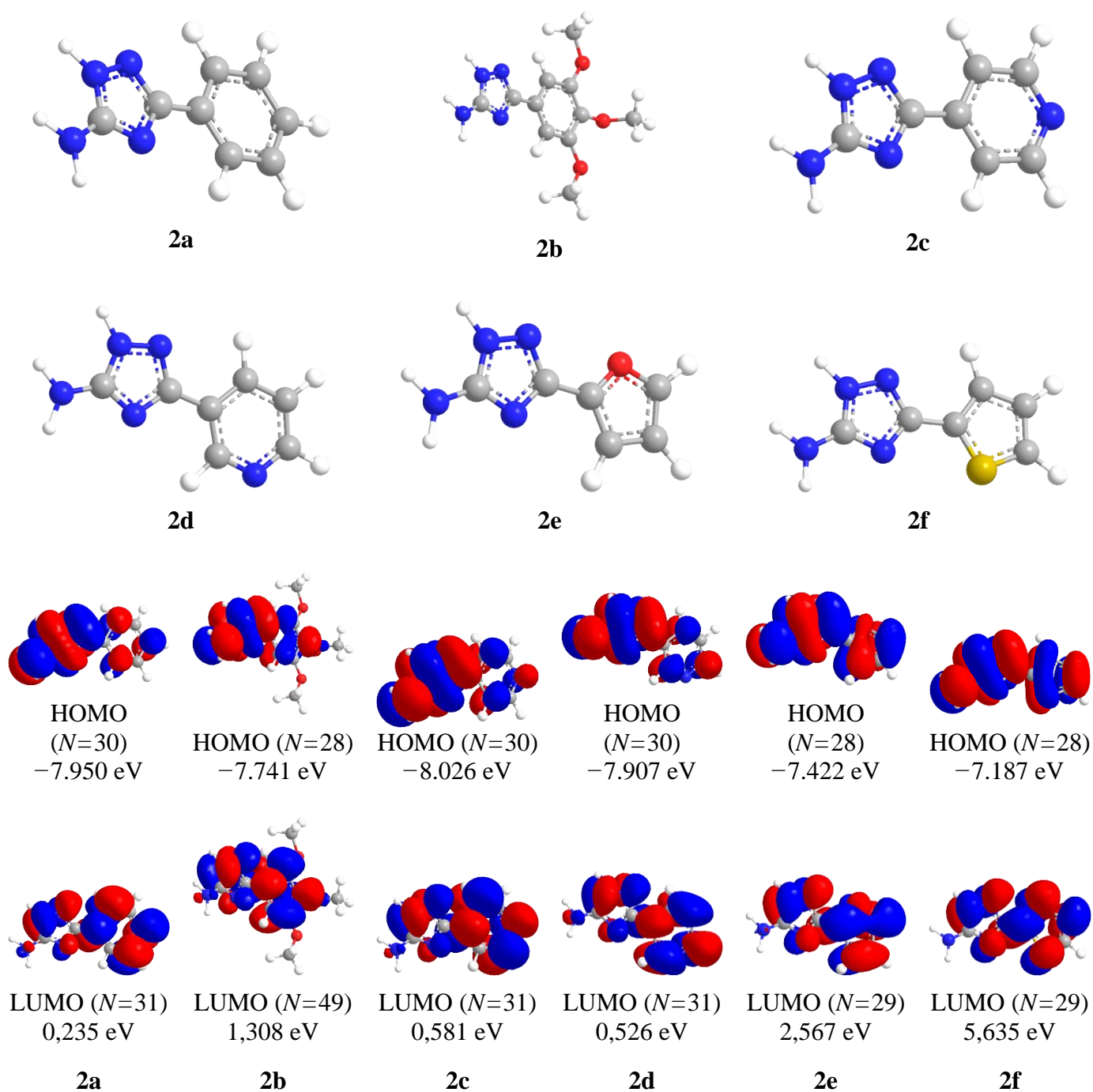
**2a**

**2b**

**2c**

**2d**

**2e**

**2f**

HOMO
($N$=30)
−7.950 eV

HOMO ($N$=28)
−7.741 eV

HOMO ($N$=30)
−8.026 eV

HOMO
($N$=30)
−7.907 eV

HOMO
($N$=28)
−7.422 eV

HOMO ($N$=28)
−7.187 eV

LUMO ($N$=31)
0,235 eV

LUMO ($N$=49)
1,308 eV

LUMO ($N$=31)
0,581 eV

LUMO ($N$=31)
0,526 eV

LUMO ($N$=29)
2,567 eV

LUMO ($N$=29)
5,635 eV

**2a**

**2b**

**2c**

**2d**

**2e**

**2f**

**Figure 2.** Optimized structures and visualization of HOMO and LUMO orbitals of inhibitors **2a**−**2f**.

**Table 4.** Calculated energies of HOMO, LUMO, HOMO-LUMO gap (HLG), ionization potential (*IP*), electron affinity (*EA*), electronegativity (χ), absolute hardness (η), and softness (σ) in eV using the B3LYP/6-31G++(d,p) basis set for compounds **2a**−**2f**.

| No. | HOMO, eV | LUMO, eV | HLG | *IP* | *EA* | χ | η | σ |
|---|---|---|---|---|---|---|---|---|
| **2a** | −7.95 | 0.235 | 8.185 | 7.95 | −0.235 | 3.8575 | 4.0925 | 0.2443 |
| **2b** | −7.741 | 1.308 | 9.049 | 7.741 | −1.308 | 3.2165 | 4.5245 | 0.2210 |
| **2c** | −8.026 | 0.581 | 8.607 | 8.026 | −0.581 | 3.7225 | 4.3035 | 0.2324 |
| **2d** | −7.907 | 0.526 | 8.433 | 7.907 | −0.526 | 3.6905 | 4.2165 | 0.2372 |
| **2e** | −7.422 | 2.567 | 9.989 | 7.422 | −2.567 | 2.4275 | 4.9945 | 0.2002 |
| **2f** | −7.187 | 5.635 | 12.822 | 7.187 | −5.635 | 0.776 | 6.411 | 0.1560 |

For a visual demonstration of the effect of introducing inhibitor 2d, scanning electron microscopy (SEM) studies were conducted. Microphotographs of the surface of copper plates were obtained before and after their exposure in a solution of inhibitor 2d, as well as photographs of them after corrosion tests in a solution of 1% HCl. The images provided (Figure 2) show that the surface of the plate (c) is heavily damaged as a result of corrosion, with numerous pits, pitting, and pores present. In contrast, the copper sample (d) exposed to a 1% HCl solution in the presence of 10 mmol/L of inhibitor 2d retained its overall surface structure, with no significant pitting observed.

Elemental surface analysis was conducted (see Table 5), according to which it can be observed that the surface of the copper sample after its exposure in aqueous solution of inhibitor 2d contains slightly higher amounts of carbon and nitrogen, indicating the deposition of the inhibitor on the surface. Tests after corrosion in a 1% HCl solution demonstrate significant loss of copper content for sample (c), as well as a substantial increase in the chlorine fraction, indicating the formation of copper chlorides. Meanwhile, for sample (d), the loss of Cu content was not as significant, with the chlorine content reaching only 1.91 at.%. These results confirm the significant inhibitory action of 3-(pyridin-3-yl)-5-amino-1,2,4-triazole **2d**.

**Table 5.** Elemental surface composition (at. %) of the copper electrode.

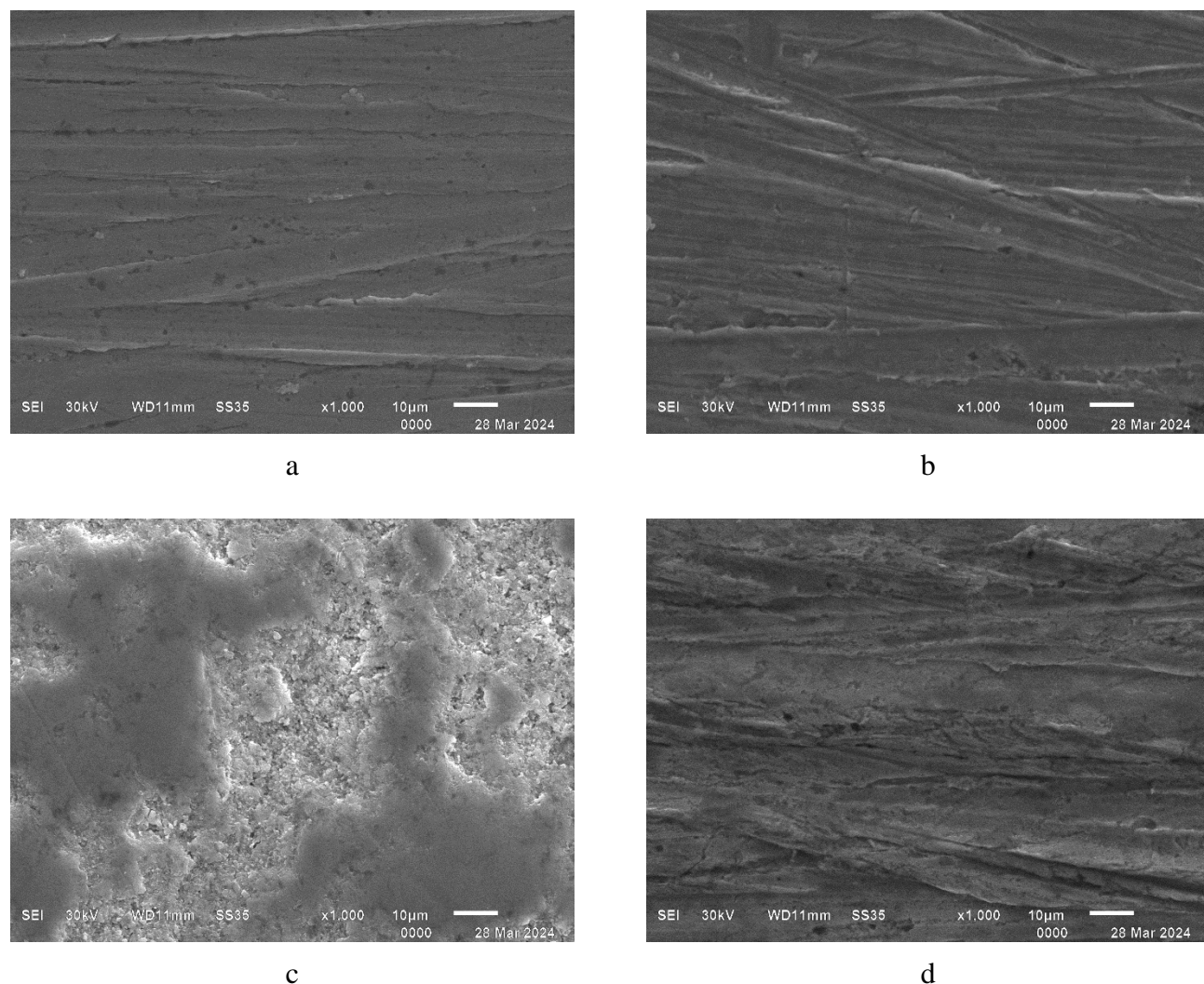| Copper plate | Cu, at.% | C, at. % | N, at.% | O, at.% | Cl, at.% |
|---|---|---|---|---|---|
| a | 92.36 | 1.65 | 3.43 | 2.56 | – |
| b | 88.30 | 4.30 | 5.26 | 2.14 | – |
| c | 60.38 | 3.03 | 4.94 | 2.57 | 29.08 |
| d | 85.05 | 4.96 | 6.65 | 1.43 | 1.91 |

**Figure 3.** SEM micrographs of the copper surface (a) before corrosion tests in 1% HCl, (b) before corrosion tests in 1% HCl +10 mmol/L inhibitor **2d**, (c) after corrosion tests in 1% HCl and (d) after corrosion tests in 1% HCl + 10 mmol/L inhibitor **2d**.

## Conclusion

As a result of the conducted research on the series of 3-aryl/hetaryl derivatives of 5-amino-1,2,4-triazole, it has been established that the corrosion inhibitory properties of substances in this class significantly depend on the structure of the aromatic substituent. Direct corrosion tests revealed that 3-(pyridin-3-yl)-1*H*-5-amino-1,2,4-triazole 2d and 3-(thiophen-2-yl)-1*H*-5-amino-1,2,4-triazole **2f** at concentrations of 0.01 M exhibited degrees of protection of 87.7% and 85.9%, respectively. These results were confirmed by potentiodynamic polarimetry. Anodic curves of these substances show a significant shift in the pitting potential, indicating a high degree of anodic process passivation on copper in the presence of the investigated compounds. On the other hand, analysis of cathodic curves showed that all tested compounds shift the region of increasing cathodic current to the cathodic area by 60–150 V. This effect increases with the concentration of the inhibitor. Thus, all investigated

compounds demonstrate a mixed mechanism of inhibition, but the most effective compounds contain substituents of pyridin-3-yl and thiophen-2-yl in their structure. All the obtained experimental results correlate well with quantum chemical calculations and are visually demonstrated in SEM studies. It is important to note that according to the results of the conducted work, the studied group of compounds possesses only moderate corrosion inhibition activity compared to existing inhibitors. However, the obtained results are important for future research on organic corrosion inhibitors and demonstrate the fundamental necessity of introducing heterocyclic substituents into their structure to enhance the protective characteristics of such compounds.

## Acknowledgments

## References

1. G. Kear, B.D. Barker and F.C. Walsh, Electrochemical corrosion of unalloyed copper in chloride media – a critical review, *Corros. Sci.*, 2004, **46**, no. 1, 109–135. doi: 10.1016/S0010-938X(02)00257-3

2. F. Ammeloot, C. Fiaud and E.M.M. Sutter, Characterization of the oxide layers on a Cu 13Sn alloy in a NaCl aqueous solution without and with 0.1 M benzotriazole. Electrochemical and photoelectrochemical contributions, *Electrochim. Acta*, 1999, **44**, no. 15, 2549–2558. doi: 10.1016/S0013-4686(98)00391-0

3. M. Finšgar and I. Milošev, Inhibition of copper corrosion by 1,2,3-benzotriazole: A review, *Corros. Sci.*, 2010, **52**, no. 9, 2737–2749. doi: 10.1016/j.corsci.2010.05.002

4. Yu.I. Kuznetsov and L.P. Kazanskiy, Physicochemical aspects of metal protection by azoles as corrosion inhibitors, *Russ. Chem. Rev.*, 2008, **77**, no. 3, 219–232. doi: 10.1070/rc2008v077n03abeh003753

5. Yu.I. Kuznetsov, Kh.S. Shikhaliev, M.O. Agafonkina, N.P. Andreeva, I.A. Arkhipushkin, A.Yu. Potapov and L.P. Kazansky, Effect of substituents in 5-R-3-amino-1, 2, 4-triazoles on the chemisorption on copper surface in neutral media, *Corros. Eng., Sci. Technol.*, 2021, **56**, no. 1, 60–70. doi: 10.1080/1478422X.2020.1807087

6. Yu.I. Kuznetsov, New possibilities of metal corrosion inhibition by organic heterocyclic compounds, *Int. J. Corros. Scale Inhib.*, 2012, **1**, no. 1, 3–15. doi: 10.17675/2305-6894-2012-1-1-003-015

7. H.O. Curkovic, E. Stupnisek-Lisac and H. Takenouti, Electrochemical quartz crystal microbalance and electrochemical impedance spectroscopy study of copper corrosion inhibition by imidazoles, *Corros. Sci.*, 2009, **51**, no. 10, 2342–2348. doi: 10.1016/j.corsci.2009.06.018

8. D.S. Chauhan, M.A. Quraishi, W.B. Wan Nik and V. Srivastava, Triazines as a potential class of corrosion inhibitors: Present scenario, challenges and future perspectives, *J. Mol. Liq*., 2021, **321**, 114747. doi: 10.1016/j.molliq.2020.114747

9. E. Kabir and M. Uzzaman, A review on biological and medicinal impact of heterocyclic compounds, *Results Chem*., 2022, **4**, 100606. doi: 10.1016/j.rechem.2022.100606

10. A.I. Konovalov, I.S. Antipin, V.A. Burilov, T.I. Madzhinov *et al*., Modern Trends of Organic Chemistry in Russian Universities, *Russ. J. Org. Chem*., 2018, **54**, 157–371. doi: 10.1134/S107042801802001X

11. M. Fesatidou, A. Petrou and G. Athina, Heterocycle compounds with antimicrobial activity, *Curr. Pharm. Des*., 2020, **26**, no. 8, 867–904. doi: 10.2174/1381612826666200206093815

12. D.S. Shevtsov, Kh.S. Shikhaliev, N.V. Stolpovskaya, A.A. Kruzhilin, A.Yu. Potapov, I.D. Zartsyn, O.A. Kozaderov, D.V. Lyapun, C. Prabhakar and A. Tripathi. 3-Alkyl-5-amino-1, 2, 4-triazoles synthesized from the fatty acids of sunflower oil processing waste as corrosion inhibitors for copper in chloride environments, *Int. J. Corros. Scale Inhib*., 2020, **9**, no. 2, 726–744. doi: 10.17675/2305-6894-2020-9-2-21

13. O.A. Kozaderov, Kh.S. Shikhaliev, Ch. Prabhakar, A. Tripathi, D.S. Shevtsov, A.A. Kruzhilin, E.S. Komarova, A.Yu. Potapov, I.D. Zartsyn and Yu.I. Kuznetsov, Corrosion of α-Brass in Solutions Containing Chloride Ions and 3-Mercaptoalkyl-5-amino-1*H*-1, 2, 4-triazoles, *Appl. Sci*., 2019, **9**, no. 14, 2821. doi: 10.3390/app9142821

14. O.A. Kozaderov, Kh.S. Shikhaliev, Ch. Prabhakar, D.S. Shevtsov, A.A. Kruzhilin, E.S. Komarova, A.Yu. Potapov and I.D. Zartsyn, Copper corrosion inhibition in chloride environments by 3-(*N*-hetaryl)-5-amino-1*H*-1, 2, 4-triazoles, *Int. J. Corros. Scale Inhib*., 2019, **8**, no. 2, 422–436. doi: 10.17675/2305-6894-2019-8-2-19

15. A.A. Kruzhilin, D.V. Lyapun, D.S. Shevtsov, O.A. Kozaderov, A.Yu. Potapov, I.D. Zartsyn, Ch. Prabhakar and Kh.S. Shikhaliev, New [1, 2, 4] triazolo [1, 5-a] pyrimidine-7-one corrosion inhibitors for copper in chloride environments, *Int. J. Corros. Scale Inhib*., 2021, **10**, no. 4, 1474–1492. doi: 10.17675/2305-6894-2021-10-4-7

16. A.L. Mnjoyan, *Synthesis of heterocyclic compounds*, Acad. Sci. Armenian SSR, Yerevan, 2001, **5**, 11 (in Russian).

17. T. L. Gilchrist, *Heterocyclic Chemistry*, Mir, Moscow, 1996, p. 144 (in Russian).

18. L.S. Wittenbrook, The The chemistry of N-cyanodithioimidocarbonic acid. III. An intermediate in heterocyclic synthesis, *J. Heterocycl. Chem*., 1975, **12**, no. 1, 37–42. doi: 10.1002/jhet.5570120107

19. M.J. Frisch, G.W. Trucks, H.B. Schlegel, G.E. Scuseria, M.A. Robb, J.R. Cheeseman, G. Scalmani, V. Barone, G.A. Petersson, H. Nakatsuji *et al*., *Gaussian16 Revision B.01*, 2016, Wallingford, Gaussian Inc.

20. R.G. Parr and R.G. Pearson. Absolute hardness: companion parameter to absolute electronegativity, *J. Am. Chem. Soc*., 1983, **105**, no. 26, 7512–7516. doi: 10.1021/ja00364a005

21. Ya.G. Avdeev and Yu.I. Kuznetsov, Chemical transformation of corrosion inhibitors in the aggressive environment/metal system. Review, *Int. J. Corros. Scale Inhib*., 2019, **12,** no. 4, 1751–1790. doi: 10.17675/2305-6894-2023-12-4-19

22. M.M. Antonijević, S.M. Milić and M.B. Petrović, Films formed on copper surface in chloride media in the presence of azoles, *Corros. Sci*., 2009, **51**, no. 6. 1228–1237. doi: 10.1016/j.corsci.2009.03.026

23. A. Fateh, M. Aliofkhazraei and A.R. Rezvanian, Review of corrosive environments for copper and its corrosion inhibitors, *Arabian J. Chem*., 2020, **13**, no. 1, 481–544. doi: 10.1016/j.arabjc.2017.05.021

24. A.M. Alfantazi, T.M. Ahmed and D. Tromans Corrosion behavior of copper alloys in chloride media, *Mater. Des*., 2009, **30**, no. 7, 2425–2430. doi: 10.1016/j.matdes.2008.10.015

♦ ♦ ♦